INJURY BIOMECHANICS RESEARCH
Proceedings of the Thirty-Ninth International Workshop

Development of Injury Criteria for Spleen and Kidney in Side Impacts with the Full-Body Human Model

Ning Zhang[1], Kawaguchi Hiroo[2], and Jay Zhao[1]

[1]TK Holdings Inc., USA
[2]Takata Corporation, Japan

ABSTRACT

This study was motivated from field observation of severe and fatal injuries to abdominal solid organs in side impacts, and the necessity to assess these injuries when using a full-body human model in the development of restraint system devices. The goal of this work was to develop and validate model-based injury criteria for the spleen and kidneys in side impacts.

Takata's existing in-house full-body human model was used to develop and validate the injury criteria for the spleen and kidneys. At the tissue and organ level, meshes of both the spleen and kidneys were refined, and the material models for these organs were validated against test data generated from multiple sources at different loading rates. At the whole body level, three series of post-mortem human subjects (PMHS) tests were selected for the model validations, which include Wayne State University PMHS linear side impact cases (Chung, et al. 1999), and Medical College of Wisconsin (MCW) PMHS side airbag (SAB) static and dynamic out-of-position (OOP) test cases (Hallman, et al. 2010). To quantify the SAB loading, a generic SAB model in MCW's OOP tests was characterized according to the MCW setup (Hallman, et al. 2009) with the same level of deployment energy and the same airbag volume and dimensions. The PMHS test validation results showed very good correlation with the force-displacement corridors developed from the existing literature for the spleen and kidneys. Chest deformations at the Axilla, Xyphoid, and T10 level were validated against chest band measurements, as were accelerations at T1, T12, and the sacrum. Finally, forces from rigid loading plates at the thorax, abdomen, and pelvis regions were all validated against the tests.

To develop the injury criteria for the spleen and kidneys, different measures for the tissue injuries were evaluated against the selected PMHS test data, including: principal stress, principle strain, and strain energy density (SED). It was found that the tolerances of the stress and strain-based injury measures varied widely with the PMHS test set-up, loading conditions, and modeling methods. Comparatively, peak SED showed much less variability and therefore SED is proposed as the indicator of injury risk for

both the spleen and kidney. The injury thresholds for the spleen and kidney are 35KJ/m^3 and 27KJ/m^3, respectively, for the current study, which are consistent with both the tissue-level material test data reported from the literature and the PMHS full body side impact tests.

INTRODUCTION

According to field data analysis using NASS and CIREN database (Klinich et.al, 2010), half of AIS 2+ abdominal injuries were from side impact accidents, and because of the anatomical location of spleen and kidney in the abdominal region, these two organs are among the most frequently injured solid organs in nearside impact cases. Another field data report showed that among 5404 side impact cases from NASS, 24% of AIS 4-6 injuries were from abdominal region. For near side impact from left side, kidney and spleen were most frequently injured, and for near side impact from right side, liver and kidney were most frequently injured organs in the abdominal region (Rouhana and Foster, 1985). To develop countermeasures or advanced restraints for mitigating such injuries from the field it requires our better understanding of the injury mechanism and having better injury assessment tools especially for the solid organs.

The spleen lies on the left side of abdomen between the 9th and 11th ribs, and its costal surface is convex to fit the chest wall. Its diaphragmatic surface is convexly curved to fit the concavity of the diaphragm. The anterior and superior borders are sharp and notched, while the posterior and inferior borders are rounded. The kidneys lie retroperitoneally on the posterior abdominal wall, one on each side of the vertebral column at the level of T12 to L3 vertebrae. The right kidney lies at a slightly lower level than the left one (Moore and Agur, 1995). Because the anatomical asymmetry of the abdominal organs, current anthropomorphic tests devices (ATDs) with symmetrical abdominal structure without details of individual organs can not differentiate the directional risks of impact, and injuries of individual organs. A whole human body mathematical model with detailed organs and appropriate assessment method for the injuries would provide more insights and understanding of injury risk and mechanism of kidney and spleen under side impacts, and thus aid development of advanced restraint systems.

In-house developed Takata Human Body Model (TKHM) represents a 50 percentile adult male. The model was previously validated with 45 sets of PMHS body impact data and 5 sets PMHS sled test data (Zhao and Narwani, 2007). However, to use it for injury assessment for the kidney and spleen, the model was subject to further development. The scope of this study included the following:

- The human organs model refinement and additional full body model validations against three series of post-mortem human subjects (PMHS) test data of side impacts in the chest and abdominal regions—Wayne State University PMHS linear side impact cases (Chung, et al. 1999), and Medical College of Wisconsin (MCW) PMHS side airbag (SAB) static and dynamic out-of-position (OOP) test cases (Hallman, et al. 2010).
- Investigation of meaningful tissue injury indicators and the model based tissue level failure thresholds.

METHODS

Geometry and meshing

To improve the stress-strain characteristics of the organ model, the mesh of spleen and left kidney were refined upon the original model. The average mesh size of spleen and kidney was decreased from 10mm to 4mm in the current study. The interfaces between spleen, kidney and surrounding organs (diaphragm, posterior abdominal wall, pancreas, intestine etc.) were carefully examined to prevent any nodal penetration between tissues. For efficiency and stability, 8-node solid element with 1 point integration and default hourglass control was selected as tissue element type.

Material property of spleen and kidney tissues

In the current study, the materials for spleen and kidney were simplified and assumed to be isotropic and homogeneous, and a nonlinear viscous material law (Ls-Dyna MAT_62) was used to represent the nonlinear and viscous (rate-dependant) behavior of the material. The model consists of a nonlinear stiffness in parallel with a viscous damper. The elastic stiffness resists the total volume crush, and viscosity generates the shear stresses. The input parameters for spleen were based on studies by Lee and Yang (2001). Farshed et al (1998) tested fresh pig kidney tissues using cubic specimens (10x10x10mm). The specimens were harvested in tangential longitudinal direction (superior-inferior), and radial direction (medial-lateral). The compressive material tests were conducted under four different loading rates (1mm/min, 10 mm/min, 100 m/min, and 500 mm/min) which were all in quasi-static ranges. The data from the highest loading rate of specimens harvested from both radial direction and longitudinal direction were selected for correlation of material model. Snedeker *et. al.* (2004) tested 45 pork kidney samples in cylindrical shape (11, 20, or 30 in diameter, and 7-9 in thickness) under a compressive loading. The specimens were harvested along sagittal plane. The dynamic loading rates were up to 25m/s. Test results with the highest loading rate from Snedeker's data were selected to validate the rate effects.

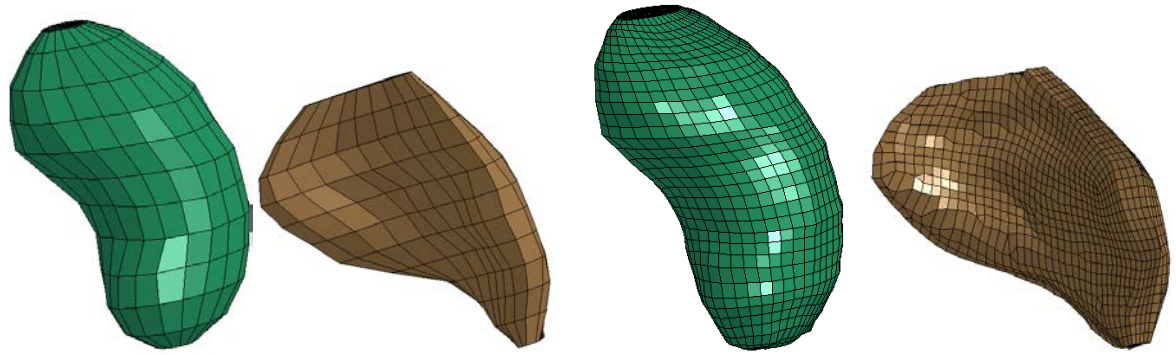

Before After

Figure 1 The mesh of spleen and kidney were refined and mesh size were reduced from an average of 10mm to 4 mm.

A compressive material test was simulated to determine the material input parameters. As shown in Figure 2, a specimen with a square cross section (20mm x 20mm) and a height of 30mm was modeled. The symmetric boundary conditions were applied to one end, while the other end was compressed by a rigid plate. The friction coefficient between the loading plate and specimen was assumed to be zero to

represent the ideal compression test condition. Loading rate was assigned to be 2.5 1/s for low strain rate cases, and 250 1/s for high strain rate cases. For efficiency and stability, 8-node solid element with 1 point integration and default hourglass control was selected as element type. The average size of element was kept as 4mm.

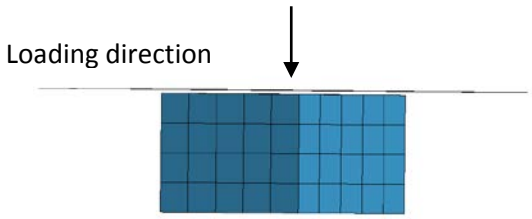

Figure 2 Kidney tissue material testing simulation and results

Organ level validation for kidney

Once tissue material property of the model was determined, organ level validation for the kidney model was conducted with the test data for vivo monkey kidneys by Melvin et al (1973). A rigid cylindrical impactor with a diameter of 38mm at a speed of 2.5m/s impacted into the kidney organ model. The force deflection curve was plotted and compared with the test corridor.

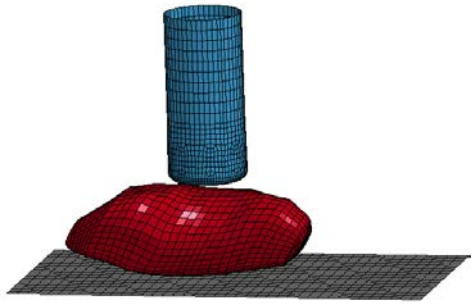

Figure 3 Simulation setup for organ level validation of kidney model based on Melvin *et. al.* (1973).

Whole body validation based on PMHS side impact tests with impactors (Chung *et al*, 1999)

To improve bio-fidelity of the torso of TKHM under side impact loadings, a set of linear impactor tests using PMHS conducted by Chung et al. (1999) were selected for model validation. An impactor with a weight of 50 kg, and a diameter of 152mm (6 in.) was accelerated to a speed of 5.6 m/s before impacted into right side of torso at T6 level. The stoke of this impactor was 50mm after the initial contact. Chest bands for chest deflection measurement were instrumented at T6 level of chest, and tri-axial accelerometers were mounted on the vertebrae at T1, T6, and T12 level, on the surface of sternum at T6 level. Results from 4 unpadded PMHS tests were used for model validation, and all result data were scaled to 50th percentile of adult male. The kinematics from high speed video, results of chest band, and spine/sternum acceleration were compared with model prediction.

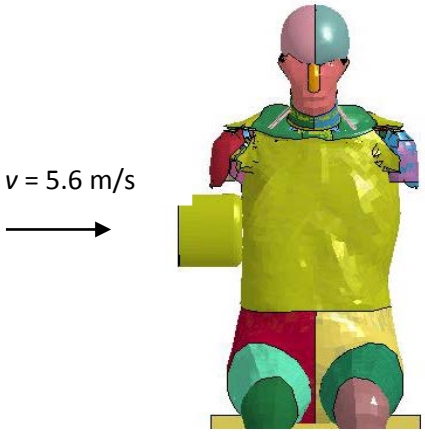

Figure 4. Model setup according to WSU linear impactor side impact tests.

Whole body validation based on PMHS side impact tests with side airbags and rigid walls (Hallman *et al* 2010)

The TKHM was further validated against the PHMS tests conducted by Hallman *et. al.* (2010) with side airbags (SAB). In their test, a SAB module with a volume of 11 liters and a size of 44 cm along median-lateral direction of the torso, and 40 cm along superior-inferior direction of torso was used, and the bag deployment force was quantified with deployment of bag against a load cell instrumented flat and rigid surface. To achieve the same impact force and energy, a generic SAB model with the same volume and dimension was tuned with the load cell output. A good correlation of force rising rate and peak force was obtained (Figure 5).

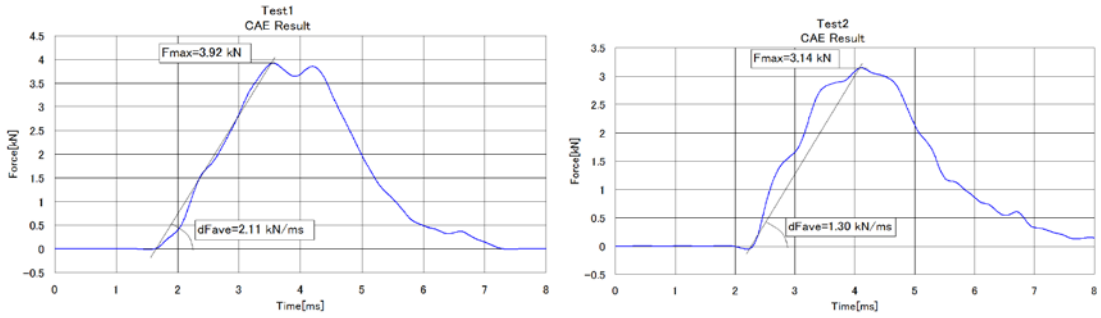

Figure 5. Validation of airbag forces with static deployment againt a rigid wall instrumented with load cells: expansion force along cushion main surface direction (test 1) and protusion force along SAB deplyment path (test 2).

Two types of loadings were applied to PMHS: in static cases seated PMHS were positioned adjacent to a rigid wall and distance between SAB module and posterilateral thorax was 1cm; in dynamic cases the rigid wall impacting towards the PMHS at a speed of 6.7 m/s while SAB deployed when the gap between torso and rigid wall was 150mm. The SAB model was positioned vertically between T6 and L1 level. The rigid wall was instrumented with three load cells to measure the impact force at regions of thorax, abdomen, and pelvis. Chest bands were mounted at Axilla, Xyphoid, and Rib 10 levels. Tri-axial

accelerometers were mounted on vertebrae at T1, T12, and Sacrum levels. Both static and dynamic SAB loading test setup were simulated with TKHM (Figure 6), and the calibrated SAB model. The outputs of simulation (chest band, thorax, abdomen and pelvis force, spine acceleration) were compared with test data.

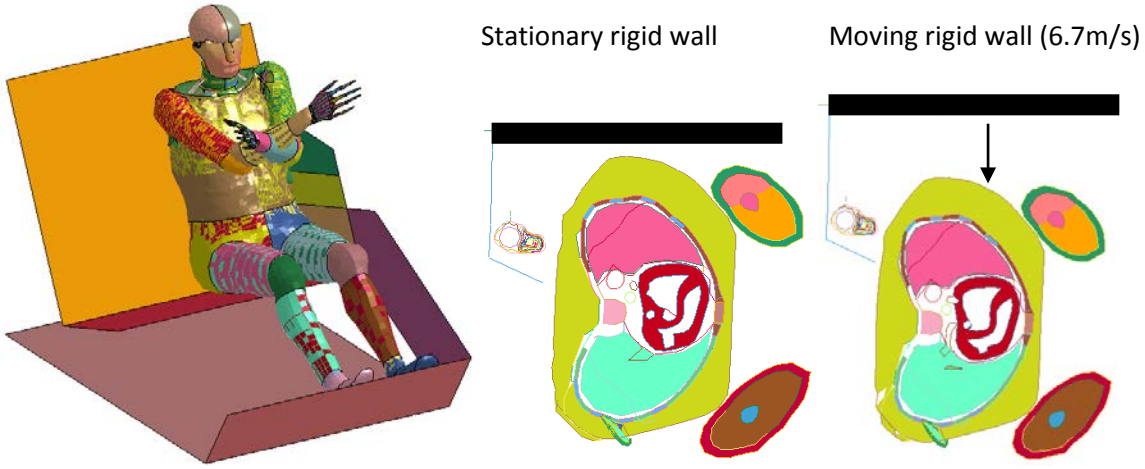

Figure 6 Simulation setup for SAB loading with stationary wall and moving rigid wall.

Development of model based injury criteria for spleen and kidney

Injuries identified from necropsy, including rib fractures and spleen and kidney lacerations, were analyzed and summarized from 4 PMHS of WSU tests (Chung et al 1999), and 7 PMHS of MCW tests (Hallman et al, 2010). Peak Von-Mises stresses of cortical shell elements from ribs, peak principal strain, principal stress, and strain energy density of elements representing spleen and kidney tissues were calculated from each loading case. Peak values were compared with threshold values of tissue failure reported from tissue level material tests. The best injury predictor was selected based on the indicator's capability of prediction of injury severity, and if the predicted values agree with tissue level failure thresholds.

RESULTS

Results on correlation of material properties of kidney tissue

After the appropriate material input parameters for stiffness and rate effects were determined, the predicted strain-stress curve of the kidney tissue under a compressive test correlated with both quasi-static and dynamic loading rate cases (Figure 7a). After plugging in the correlated material model to a whole kidney organ setup, the predicted results fit into the corridor of tests except for slight over-prediction in the initial toe region (Figure 7b).

Results on correlation with linear impactor side impacts

Good correlations were found for overall kinematics of PHMS motion and chest deformation indicated by chest band contours (Figure 8). Both the peak value and phrase of acceleration time-history plots of vertebrae acceleration at T1, T6, T12, and sacrum level were within the corridors of test results. Good overall correlation would ensure the corrected boundary conditions for internal abdomen organs impact behaviors.

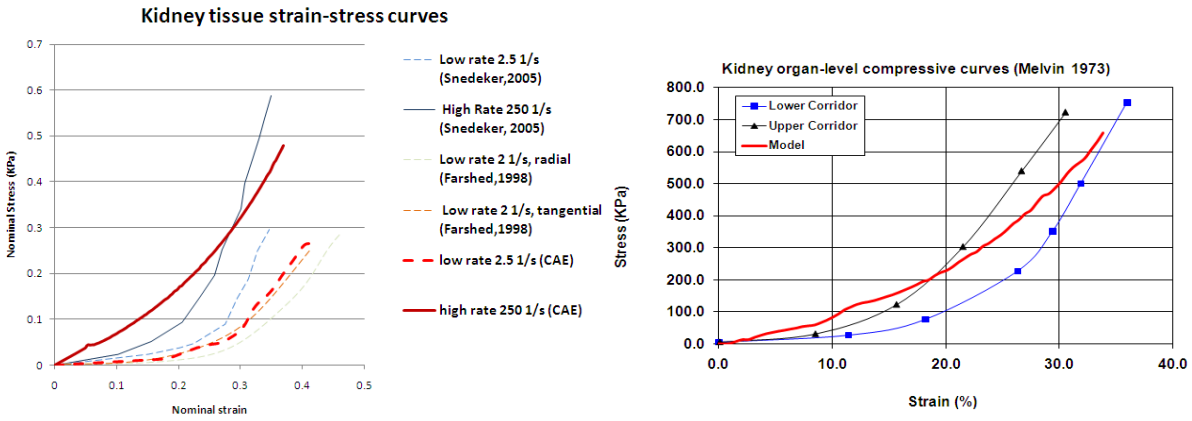

(a) **(b)**

Figure 7 Correlation results for material properties of kidney tissue: (a) tissues level test correlation; (b) organ level test correlation.

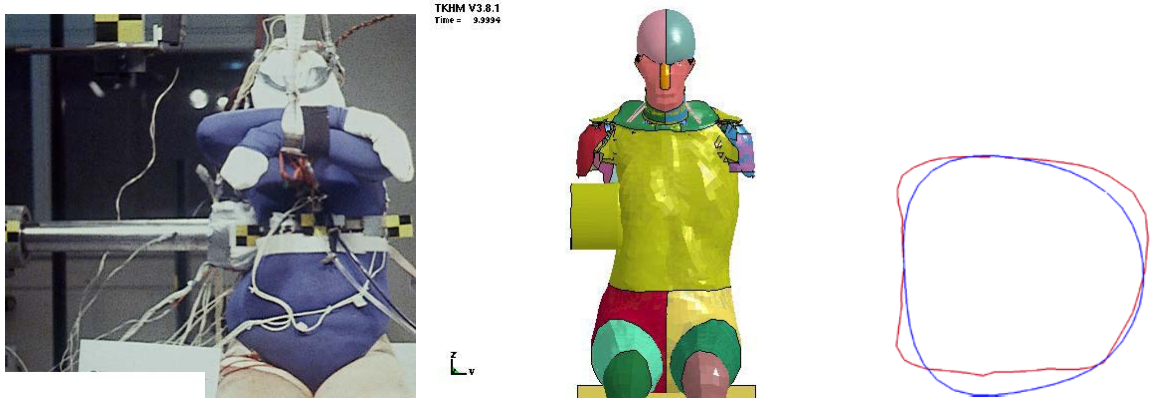

10ms

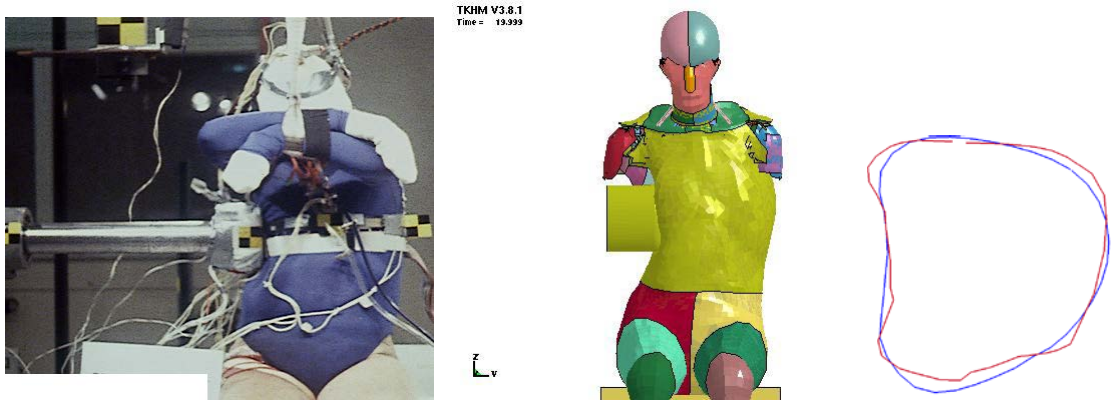

Figure 8 Kinematics and chest band comparison between test and simulation (blue lines: chest band output from tests, red lines: chest band output from simulation).

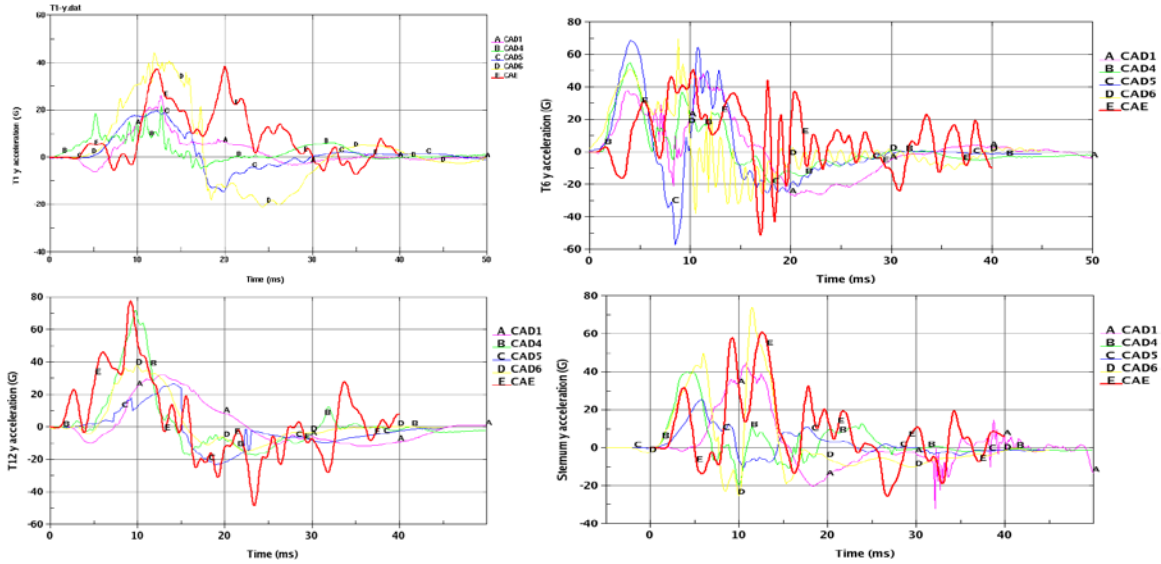

Figure 9 Correlation results for lateral accelerations of T1, T6, T12 and Sacrum level for impactor side impact cases.

Results on simulation of PMHS under SAB loading

Simulation results for both static and dynamic cases showed very good overall correlation. Detailed outputs for dynamic cases were reported here. Figure 10 showed the impact force correlation for thorax, abdomen and pelvis: despite slight over prediction of thorax and pelvis peak forces, most of the force time-history curves fit into the test curve corridors. Figure 11 showed the chest band output vs. the angle in a polar coordinate system (original point at center of chest cross section, zero degree starts with sternum at anterior posterior direction, Hallman, 2010). Good chest band correlation was found at rib 10 level, and slightly under prediction of rib deflection at posterior region between 110 degrees to 140 degrees of xyphoid level. Figure 12 showed good correlations for vertebrae accelerations at T1, T12 and sacrum levels.

Results for injury criteria development for rib fracture and spleen, kidney laceration

Table 1 showed a good general trend of rib fracture prediction using a previously developed criterion (peak von Mises stress of 125 MPa, Zhao and Narwani, 2007). A slight under-prediction of rib fractures was expected since the average age of the PMHS was much higher than the age of the population that the current model represents. Table 2 (a-c) showed the summary of injury risks of spleen and kidney organ under three loading cases. There was no injury reported from impactor side impact cases for spleen and kidney. Only 1 splenic laceration reported out of three cases for static SAB loading. For dynamic SAB loading cases, 2 out of 4 were reported with splenic lacerations and 1 out of 4 was reported with kidney laceration.

When plotting the predicted peak kidney strain energy density (SED), peak first principal strain and stress for three loading cases with different injury risks (Figure 13), predicted peak principal kidney strains failed to predict the trend of risk. When compared with tissue level failure values reported by Snedeker et al (2005), the peak SED showed good agreement, while the strains were over-predicted, and the stresses were under-predicted. Overall, SED of 27 KJ/m^3 was selected as injury threshold for kidney in the current model.

When plotting the predicted peak spleen strain energy density (SED), peak first principal strain and stress for three loading cases with different injury risks (Figure 14), predicted peak principal spleen stresses failed to predict the trend of risk. When compared with tissue level failure values reported by Tamura et al (2002), the strains showed under-predictions, the stresses showed over-predictions, and the SED were slightly over-prediction. Overall, SED of 35 KJ/m^3 was selected as injury threshold for spleen in the current model.

When SED contours were plotted for cases with injuries for spleen and kidney, high SED regions were predicted around posterior end of the spleen, and the renal area of the kidney where blood vessels are connected. These locations agreed with laceration sites reported by Hallman et al. (2010).

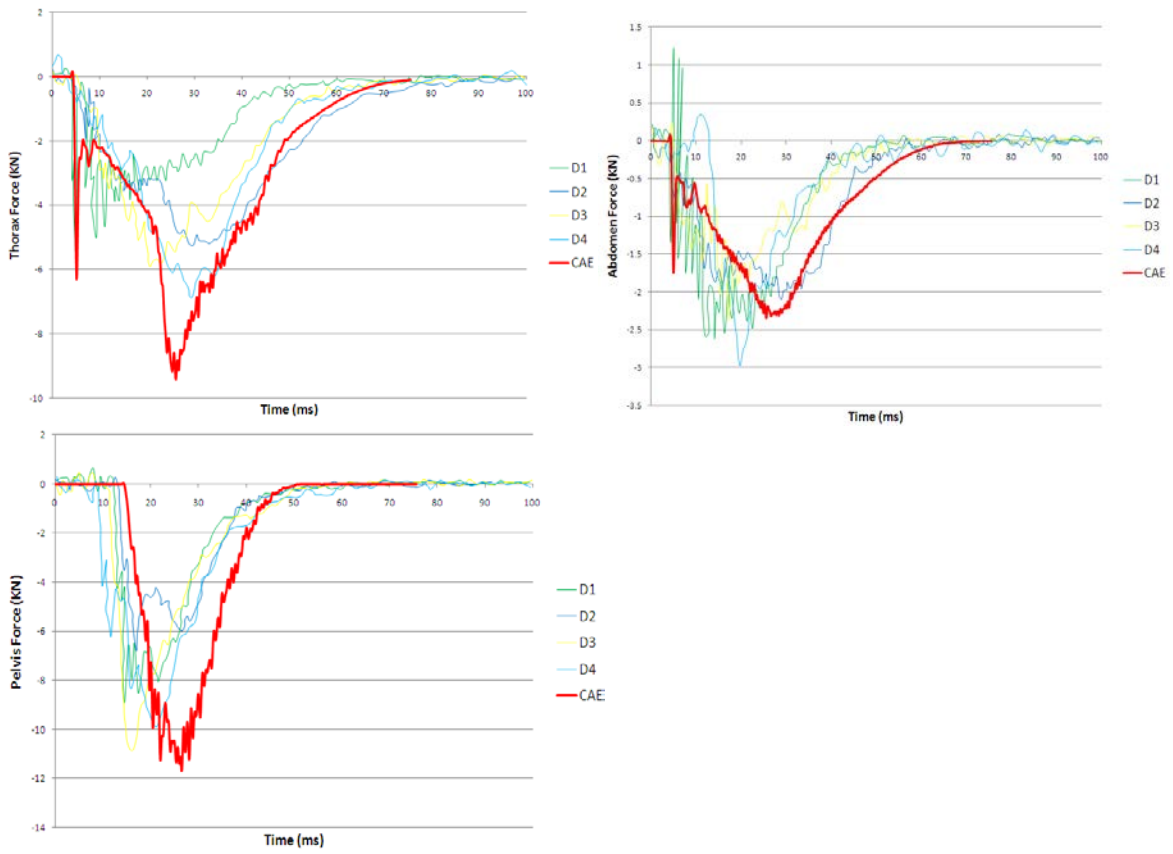

Figure 10 Correlation of impact force at thorax, abdomen, and pelvis regions for dynamic SAB loading cases.

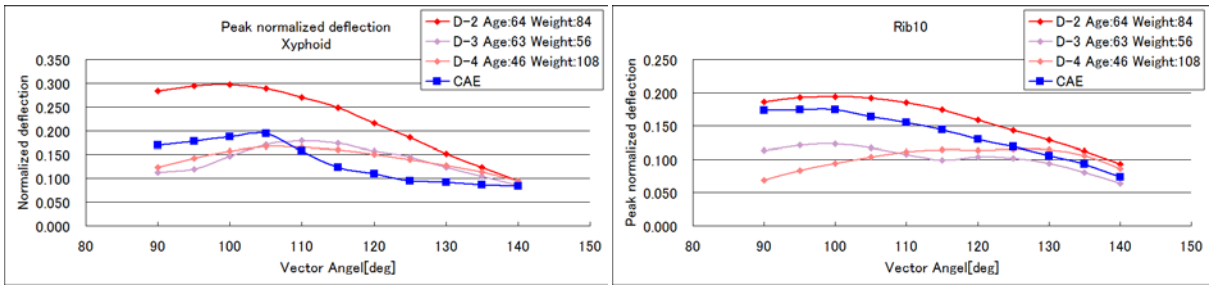

Figure 11 Correlation of chest band deflection outputs for xyphoid and T10 levels for dynamic SAB loading cases.

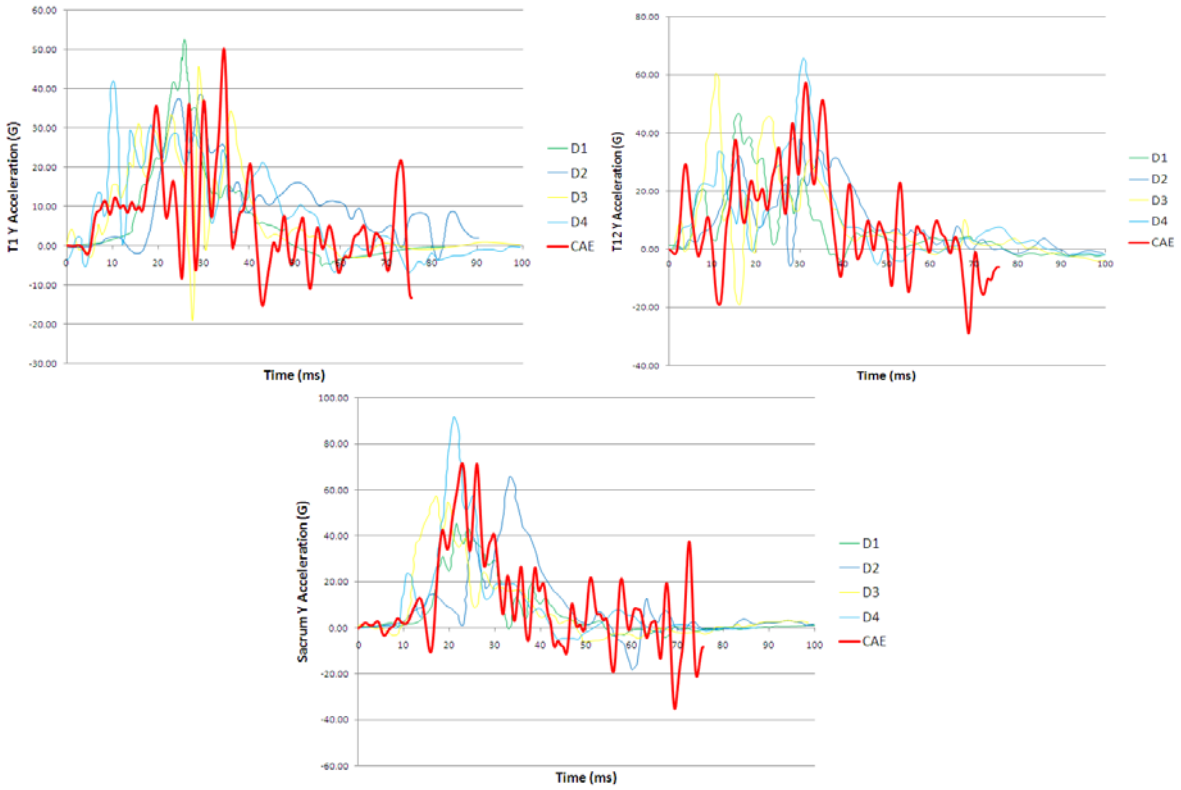

Figure 12 Correlation results for vertebrae accelerations at T1, T12 and sacrum levels for dynamic SAB loading cases.

Table 1 Comparison of reported rib fractures and model predicted fractures using the stress criteria (peak Von Mises stress of 125MPa): (a) 4 cases from WSU impactor side impact (Chung, 1999); (b) 3 cases from MCW static SAB loading (Hallman, 2010); (c) 4 cases from MCW dynamic SAB loading (Hallman, 2010).

(a)

Ribs	CAD 1	CAD 4	CAD 5	CAD 6	Model prediction
3		3	3	3	No
4		2	3	2	Yes
5	1	3	2	1	Yes
6	1	1	1	1	Yes
7	1	1	1	1	Yes
8	1	2	1	1	Yes
9		2		1	Yes
10		1			Yes
11					No
Total	4	15	11	10	7

(b)

Ribs	S-1	S-3	S-6	Model prediction
6				No
7				No
8		2	1	Yes
9		1	1	Yes
10		1		No
11		1		No
12		1		No
Total	0	6	2	2

(c)

Ribs	D-1	D-2	D-3	D-4	Model prediction
2		2			No
3	1	2		1	No
4	1	2		1	No
5	1	3			No
6	1	3			Yes
7	1	3			Yes
8	1	2		1	Yes
9		1		1	Yes
10					No
Total	6	18	0	4	4

Table 2 (a) Injury risks for spleen and kidney under impactor side impact (Chung et al, 1999)

	CAD 1	**CAD 2**	**CAD 3**	**CAD 4**	**Injury risk**
Spleen	Intact	Intact	Intact	Intact	☺ 0%
Kidney (L)	Intact	Intact	Intact	Intact	☺ 0%

Table 2 (b) Injury risk summary for kidney and spleen under static SAB loading (Hallman, 2010)

Static OOP	**S-1**	**S-3**	**S-6**	**Injury risk**
Spleen	1 Splenic lac (0.3mm)			33%
Kidney (L)				☺ 0%

Table 2(c) Injury risk summary for kidney and spleen under dynamic SAB loading (Hallman, 2010)

Dynamic	**D-1**	**D-2**	**D-3**	**D-4**	**Injury risk**
Spleen	3 splenic lac. (1.1-2.8cm)			1 splenic lac. (1.1cm)	50%
Kidney (L)		1 renal lac. (1.3cm)			25%

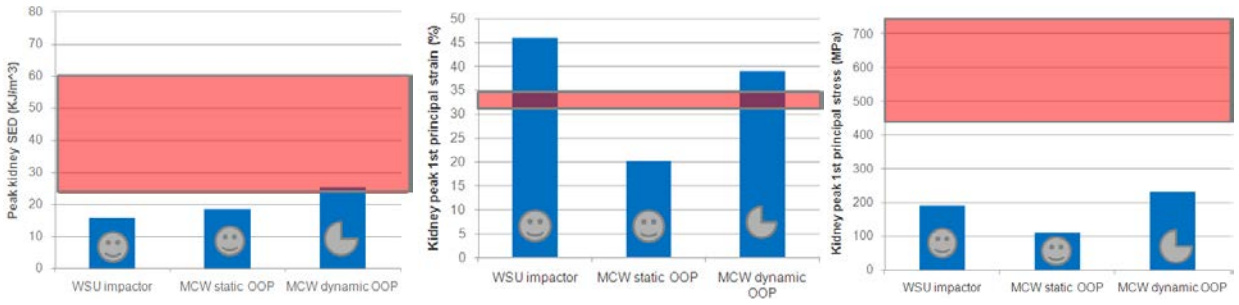

Figure 13 Predicted kidney peak strain energy density (SED), principal strain, and principal stress for three loading cases against the ranges of failure criteria from tissue level material tests (Snedeker et al, 2005).

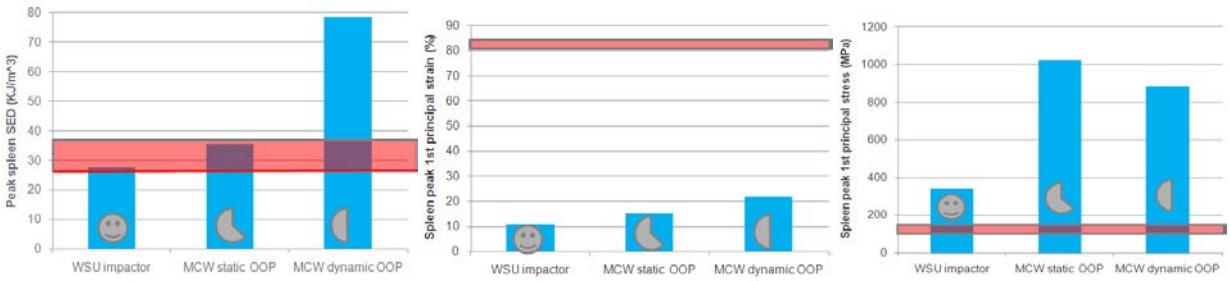

Figure 14 Predicted spleen peak strain energy density (SED), principal strain, and principal stress for three loading cases against the ranges of failure criteria from tissue level material tests (Tamura et al,2002).

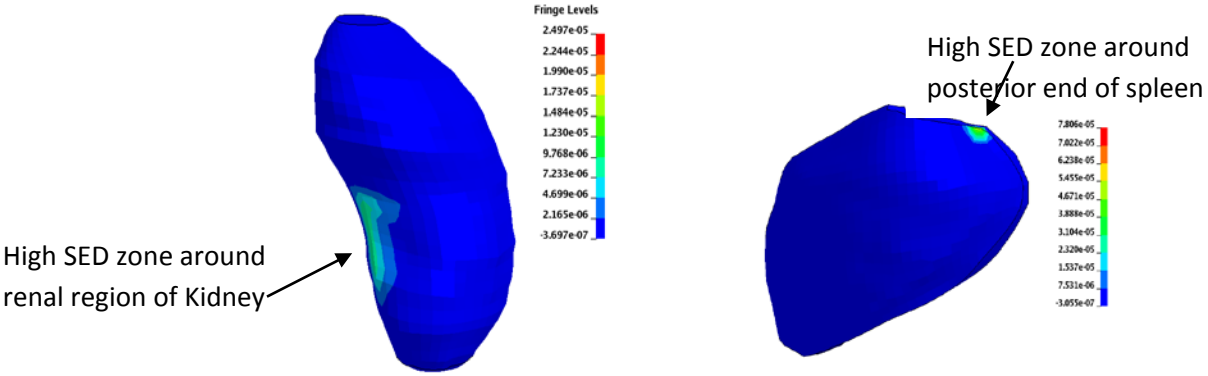

Figure 15 Predicted high SED zones which agreed with the laceration sites reported by Hallman (2010).

DISCUSSION

The current study at full body model level suggests that strain energy density is a better predictor of injury than other measures such as peak stress or strain. Its predicted values agree with tissue level failure thresholds obtained from the organ impact tests by Snedeker, J etc. (2005). Strain energy density represents the overall state of a complex deformation mode with a combination of volumetric change and shear, while the calculated strain or stress could be over-predicted or underestimated as shown in Figures 13-14 especially for more complex tissue deformation modes under severe loading in the injury scenario. Biological tissues in the physiological state are usually not unstressed (Fung et. al., 1990). Therefore, simply applying the strain threshold from tissue level of tests under uniform test conditions may not be best practice to predict the injury outcome.

This study demonstrates that for a whole body FE human model to predict tissue level injury it is critical to have a high quality geometry representation (finite element mesh including element type, element quality criteria, and hourglass control method) and clean interfaces between adjacent organs and tissues (no non-physical high stresses introduced from the contact algorithm due to nodal penetrations). Furthermore, the tissue level material property validation using the same element type, element size, and hourglass control algorithm should be performed, which provides insight of effectiveness of model setup broader than just considering of strain-stress material law itself, as the behavior of tissue in the whole body model relies on all of these parameter selections.

Biological tissues are rate sensitive. Fung (1990) pointed out that for typical biological tissues, a 1000 fold increase of strain rate would result in one fold increase in tissue stiffness. Based on the tests data from Melvin et al (1973) and Snedeker et al (2005), tissues of kidney were even more sensitive. Melvin also pointed out that static loading couldn't reproduce the injury pattern of kidney and liver seen in real-world automotive accidents. Therefore, validation of tissue material property in a high strain rate condition is important for accurate prediction of abdominal solid organ injuries. The current study didn't validate the spleen tissue with high loading rate due to lack of test data from reference. We hope to address that issue in the future once additional test data become available.

CONCLUSION

In the current study, Takata Human Body Model (TKHM) was further validated using PMHS test data under side impact scenarios. Good correlations were obtained for overall body responses such as: PMHS kinematics, chest deflection, spine and sternum accelerations, and impact forces. Solid organs of the abdominal region, especially spleen and kidney were further validated at both tissue level and organ level. The model-based peak strain energy density (SED), first principal strain and stress were evaluated as tissue level failure criteria. The SED was found to be a better injury indicator than principal strain and stress for spleen and kidney. The injury thresholds of the current model were 35KJ/m^3 and 27 KJ/m^3 for spleen and kidney, respectively.

ACKNOWLEDGEMENTS

Thanks to Dr. John Cavanaugh of Wayne State University for providing us the detailed testing data. Thanks to Dr. Jason Hallman, Dr. Frank Pintar, and Dr. Narayan Yoganandan of Medical College of Wisconsin for providing technical papers and giving suggestions to this study.

REFERENCES

CHUNG, J., CAVANAUGH, J., KING, A., KOH S. AND DENG Y. (1999) Thoracic Injury Mechanisms and Biomechanical Responses in Lateral Velocity Pulse Impacts. Stapp Car Crash Conference, SAE paper No. 99CS04.

FARSHAD, M, BARBEZAT, M, FLUELER, P., SCHMIDLIN, F., GRABER, P., AND NIEDERER, P. (1999) Material Characterization of the pig kidney in relation with the biomechanical analysis of renal trauma. J. of Biomech. Vol. 32: 417-425.

FUNG, Y., (1990) Biomechanics: Motion, Flow, Stress, and Growth. Springer.

HALLMAN, J., YOGANANDAN, N. AND PINTAR, F. (2010) Biomechanical and Injury Response to Posterolateral Loading from Torso Side Airbag. The 54th Stapp Car Crash Conference, SAE paper No. 2010-22-0012.

KINICH, K, FLANNAGAN, C., NICHOLSON, K., SCHNEIDER, L. (2010) Factors Associated with Abdominal Injury in Frontal, Farside, and Nearside Crashes. The 54th Stapp Car Crash Conference, SAE paper No. 2010-22-0005.

LEE, J. AND YANG, K. (2001) Development of a Finite Element Method of the Human Abdomen. The 45th Stapp Car Crash Conference, SAE paper No. 2001-22-0004.

MELVIN, J., STALNAKER, R, ROBERTS, V. AND TROLLOPE, M. (1973) Impact Injury Mechanisms in Abdominal Organs. Stapp Car Crash Conference, SAE paper No. 730968.

MOORE, K. AND AGUR, A. (1995) Essential Clinical Anatomy. Williams & Wilkins, Baltimore, MA.

ROUHANA, S. AND FOSTER, M (1985) Lateral Impact – an Analysis of the Statistics in the NCSS. The 29th Stapp Car Crash Conference, SAE paper No. 851727.

SNEDEKER, J., BARBEZAT, M., NIEDERER, P., SCHMIDLIN, F. AND FARSHAD, M. (2005) Strain Energy Density as a Rupture Criterion for the Kidney: Impact Tests on Porcine Organs, Finite Element Simulation, and a Baseline Comparison between Human and Porcine Tissues. J. of Biomech. Vol. 38: 993-1001.

TAMURA, A., OMORI, K., MIKI, K., LEE, J., YANG, K., AND KING, A. (2002) Mechanical Characterization of Porcine Abdominal Organs. The 46th Stapp Car Crash Conference, SAE paper No. 2002-22-0003.

ZHAO J. AND NARWANI, G. (2007) Biomechanical Analysis of Hard Tissue Responses and Injuries with Finite Element Full Human Body Model, ESV 2007 paper No. 07-0354.